Nuclear Instruments and Methods in Physics Research B 330 (2014) 24–32

Contents lists available at ScienceDirect

Nuclear Instruments and Methods in Physics Research B

journal homepage: www.elsevier.com/locate/nimb

A study of ion channeling patterns at minor axes in silicon

M. Motapothula [a,b,c,*], Z.Y. Dang [a,c], T. Venkatesan [b], M.B.H. Breese [a,c]

[a] Center for Ion Beam Applications, Physics Department, National University of Singapore, Lower Kent Ridge Road, Singapore 117542, Singapore
[b] NUSNNI-NanoCore, National University of Singapore, Singapore 117576, Singapore
[c] SSLS, National University of Singapore, 5 Research Link, Singapore 117603, Singapore

ARTICLE INFO

Article history:
Received 19 January 2014
Received in revised form 23 March 2014
Accepted 30 March 2014
Available online 19 April 2014

Keywords:
Ion channeling
Minor axes
Silicon
Crystallography
Ion implantation

ABSTRACT

We present a comprehensive study of channeling patterns showing the angular distributions of 2 MeV protons which are transmitted through a 55 nm thick [001] silicon membrane along, and close to major and minor axes. The use of such ultra-thin membranes allows the relationship between aligned and tilted patterns to be clearly observed and a correlation made between lattice geometry and pattern distribution across many axes. We study the effect of minor planes {1 1 *n*} (*n* odd) at axes which they intersect, where their changing lattice geometry results in a variety of effects. The origin of these patterns is studied with Monte Carlo simulations and we show how one may interpret aspects of the observed patterns to determine the corresponding lattice arrangement. At axes which have a single spacing between atom rows produce the well-known 'doughnut' distribution at small axial tilts. In comparison, axes which incorporate atom rows with a different spacing or geometry produce more complex channeling patterns which exhibit a secondary, inner feature produced by beam incident on these rows.

1. Introduction

Channeling occurs when energetic ions move either parallel, or nearly parallel, to an axis or a plane in a crystal [1]. Channeling causes ions to be repelled by the inter-atomic channel potentials, steering them away from the rows and planes of atoms into the open channels between the rows or planes of atoms. Channeled ions interact with the electron clouds along the channel, resulting in a smearing of their angular distribution which becomes more pronounced with increasing crystal thickness. Lindhard [2] derived formulae for the axial and planar channeling critical angles by introducing stable trajectories which considered that the ions do not come closer than the Thomas–Fermi screening radius, *a*, to the atomic rows or planes in order to be channeled. If they approach closer than this then they become either quasi channeled or randomly scattered [3].

The channeling critical angle, Ψ_c, for row of atoms in the axial case is:

$$\Psi_c = \sqrt{\frac{2z_1z_1e^2}{4\pi\varepsilon_0 Ed}}\left|\ln\left(\frac{Ca}{\rho t}\right)^2 + 1\right|^{\frac{1}{2}} \text{(radians)} \quad (1)$$

$$a = 0.8853a_0\left(Z_1^{\frac{1}{2}} + Z_2^{\frac{1}{2}}\right)^{-\frac{2}{3}} \quad (2)$$

Most studies of channeling phenomena were reported along major axes where the wide, open channels have large critical angles and longer channeling depths. Very few studies have been conducted along high Miller index (minor) axes, where the narrow channels result in smaller critical angles and rapid dechanneling due to interactions with denser electron clouds as well as shallower inter-atomic potentials. These studies were mainly conducted to complement the understanding of ion implantation effects, because channeling of low energy (<50 keV) implanted ions, such as boron and phosphorus, significantly alters the depth distribution of the implanted ions [4,5] and so the device performance. Ref. [6] experimentally located several high and low Miller indices axial/planar channels in a Si crystal for boron and helium ions in a backscattering mode. However, there remains an uncertainty as to whether perfect random alignment is achieved since there may still be a certain channeling effects.

Fig. 1 provides a guide to the angular location of the axes and planes around the Si [001] axis as relevant to the present study.

2. Transmission channeling

In axial alignment, channeling patterns produced by the transmitted beam passing through thick crystals (greater than a few hundred nanometers) resemble a star [7,8] having bright

* Corresponding author at: Center for Ion Beam Applications, Physics Department, National University of Singapore, Lower Kent Ridge Road, Singapore 117542, Singapore. Tel.: +65 83086250; fax: +65 67776126.
E-mail address: malli@nus.edu.sg (M. Motapothula).

http://dx.doi.org/10.1016/j.nimb.2014.03.021
0168-583X/

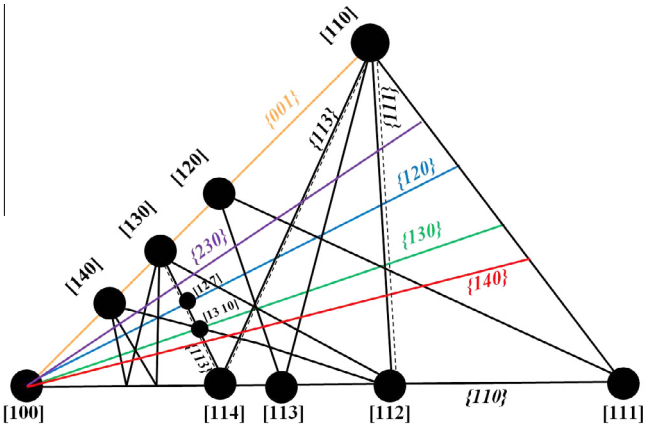

Fig. 1. Stereographic projection of axes and planes in Si lattice along ⟨001⟩, showing the major and minor axes and planes considered here.

regions in the middle, and showing blocking regions along the planes of intersections [1], which can aid the location of an axis. The transmission mode of observing channeling phenomena [9–11] has an advantage in several respects, where one can clearly visualize the angular location of the lattice or image any crystalline defects present such as dislocations and stacking faults, along with observing effects of oscillatory behavior in planar alignment [12,13].

It is now feasible to prepare perfectly crystalline ultra-thin silicon membranes which are only 55 nm thick [14,15]. A description of our sample fabrication and experimental details for fabricating ultra-thin silicon membranes is given in Ref. [14]. Recording such channeling patterns using a simple detection system comprising a YAG scintillator screen and a video camera requires less than a second per image, allowing a wide range of pattern variations from major and minor axes to be compiled under different tilt conditions.

Channeling patterns produced from thick crystals such as the silicon [001] and [111] axes exhibit ring-like shapes on tilting the crystal slightly away from a major axis [16–19] often referred to as "doughnuts", the diameter of the ring increases with tilt angle away from alignment [14]. However, when the crystal is thin (100 nm or less), the axial patterns are more complex [20,21], containing much fine-scale structure arising from the non-equilibrium trajectories which cannot be seen from thicker crystals due to multiple scattering with electrons [22]. For small tilts one observes strong variations from the ring-like shape, in which they appear as geometric shapes such as square and hexagon depending on the axis and the beam tilt [21,23]. For the [011] axis there is additional central feature observed in recorded patterns [21] and simulations [24]. It was previously referred to as the inner of two doughnut distributions.

Here we present a compendium of various pattern shapes and symmetries at minor axes, building on our earlier work [20] where we observed asymmetric axial channeling patterns from axes along the {111} planes, on tilting between the [112] and [110] axis, such as the [213] and [314] axes. The wide {111} plane produced a symmetric pattern both at axial alignment and for a small tilt away, whereas the narrow {111} plane produced an asymmetric pattern owing to the offset between its atom rows.

For materials such as silicon with a diamond crystal structure, all of the {1 *m n*}, *m*, *n* = odd, set of planes have two widths, referred to as wide and narrow. The {111} is the widest among them all, and also it is the only plane where the atom rows of wide channels are opposite each other. Other planes in this family, such as the {113}, also have two widths and since the row atoms of the wide channels are not opposite at most axes which intersect these planes, then one might expect the channeling pattern produced by the wider planes to be asymmetric, as well as that from the narrow planes.

The aims of this study are as follows. First, to provide a compendium of the different channeling patterns observed at various major and minor axes as a reference source, both at axial alignment and for small tilts away. Second, to study the relation between observed pattern asymmetry and the crystal lattice arrangement at minor axes. Finally to derive a generalized behavior across different lattice directions, allowing us to elucidate details of the lattice structure from certain observed pattern attributes.

3. Results

3.1. Axes along major planar directions

Fig. 2a shows a composite set of calculated maps of static interatomic axial continuum potentials, $V(r)$, at various axes using the ZBL universal potential [25], along with the corresponding axially aligned channeling patterns in Fig. 2b, from Ref. [18]. Previously we reported the aligned and tilted case for channeling patterns mainly at major axes [001], [011] and [111] in Refs. [14,20,21]. Here we show the corresponding doughnut patterns obtained from tilting either along, Fig. 2c, or perpendicular to the major planes {001}, {011} and {111}, Fig. 2d, at axes along these directions. One needs to bear in mind that the patterns shown for the [001], [112] and [011] axes (i.e. those at each corner of the triangle) can be considered to be interchangeable between Fig. 2c and d depending on which set of intersecting major planes one is considering, hence both are included in each figure. An initial observation is that each doughnut pattern may exhibit a unique shape, or one that is similar to that observed at other axes, depending on whether the basic atomic arrangement is similar.

Fig. 3 shows a more detailed observation of the evolution of the channeling patterns at the [014], [013] and [012] axes for increasing tilts parallel to (columns a, c, e) and perpendicular to (columns b, d, f) the {001} direction. Fig. 4 similarly shows more detailed evolution of the channeling patterns at the [114], [113] and [112] axes for increasing tilts parallel to (columns a, c, e) and perpendicular to (columns b, d, f) the {011} direction.

3.2. Axially aligned patterns along minor planar directions

Section 3.1 presented channeling patterns which were recorded at axes along major planar directions. We now consider the effect of tilting along minor planar directions, specifically {012} in Fig. 5, {013} in Fig. 6 and {113} in Fig. 7 to provide a comprehensive overview of the relationship between the lattice geometry, mirror symmetry and the observed channeling pattern. Each figure shows an axially aligned pattern at minor axes encountered along a certain planar direction, along with the corresponding FLUX [24] simulated pattern and the atomic arrangement. FLUX is a widely-used Monte Carlo simulation programme for ion channeling, it combines the binary collision model and multi-string approximation, as well as the nuclear and electronic stopping as a function of impact parameter. Where the lattice is symmetric we denote this as 'S' and show the mirror symmetry planes in dashed lines. Note that most of the axes are asymmetric along these directions, as are the corresponding channeling patterns.

4. Analysis and discussion

4.1. Tilts parallel to a major planar direction

Consider the following pattern sequence in Figs. 2–4, starting from [001] to [114] to [012] to [113] to [014]. This sequence

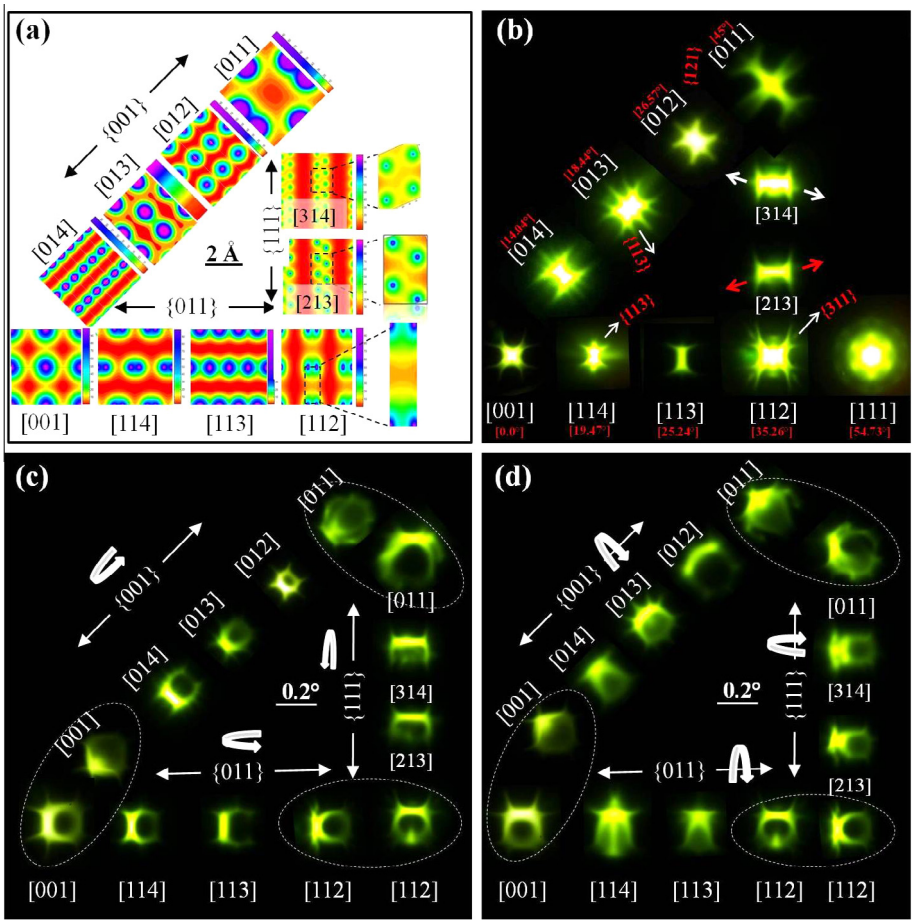

Fig. 2. (a) Collage of static atomic potentials averaged along the ion direction at different axes away from the [100] axis, at angular locations shown in red along (001), (011), (111) planar directions. Red/violet regions represent low/high potential in the scale bars at each map, (b) experimental channeled angular distributions at aligned cases for 2 MeV protons from a 55 nm [001] Si membrane, doughnut channeling patterns (c) tilting along the planes and (d) perpendicular to the planes. All pictures are for different exposures to best highlight features in each. (For interpretation of the references to color in this figure legend, the reader is referred to the web version of this article.)

of axes is not specific to one tilt plane as the purpose is to consider those axes which provide a suitable set for observing the trend from a potential distribution which is modulated strongly in two dimensions where the potential due to each atomic string is clearly resolved and ions may freely move between adjacent atomic strings, to a higher index axes which is intersected by only one major plane. In this case there is a linear region of low potential which is bounded by more continuous potential walls, through which ions may pass with difficulty. In the potentials in Fig. 2a, there is a progression from lattice walls which are very open at a major axes, i.e. [001] to axes, to a lattice potential which is more continuous at the [114] and [012] axes, which still has valleys in the potential walls through which one might consider that ions may move, though less readily than at the [001] axis, to axes where the lattice potential becomes more continuous and uniform, such as the [113] and [014] axes. Note that the [114] potential contains two closely-spaced atoms which give rise to other effects discussed later where tilts perpendicular to them are considered.

At a major axis, tilting away from axial alignment results in a channeling pattern which exhibits a continuous, ring-like doughnut structure in Fig. 2c and d. Whether this is a square shape at [001], or a hexagonal shape at [114] and [012] depends on the corresponding atomic arrangements [21]. The origin of such doughnut distributions has been studied [23]; trajectories along a major axis acquire a range of azimuthal angles owing to moving through the regions of low potential into adjacent unit cells. For the [114] and [012] axes, apart from the hexagonal shape observed to the right, one observes a strong, curved, cusp-shape to the left, produced by ions which move through gaps in the lattice potential into an adjacent channel. For the [113] and [014] axes, a weaker, less continuous doughnut distribution is observed, consistent with more continuous potential wall through which ions have a lower probability of passing. The more confined nature of their resultant motion within a one dimensional potential results in behavior similar to planar channeling with a less-continuous doughnut distribution.

4.2. Tilts normal to a major planar direction

Consider the similarities between the channeling patterns in Figs. 2–4 which are observed on tilting perpendicular to the widest intersecting plane (this may be either a {001} or {011} plane), for the cases of the [012], [014] and [113] axes. These have similar hexagonal-shaped lattice arrangements and lattice potentials with regularly-spaced atoms, though with different degrees of openness along the atomic strings. The similarity of their patterns on tilting, particularly for a tilt of $\sim\psi_c/2$ is obvious, they all exhibit doughnut-like patterns, though vary a little in the degree to which complete rings are observed for the more open axes (e.g. [012] axis) compared to incomplete rings for more closed axes. At these axes the lattice direction in which the beam is tilted comprises atom rows with the same offset geometry.

The tilted channeling patterns observed at the [114] axis in Fig. 4b exhibit a more complex structure than those from the

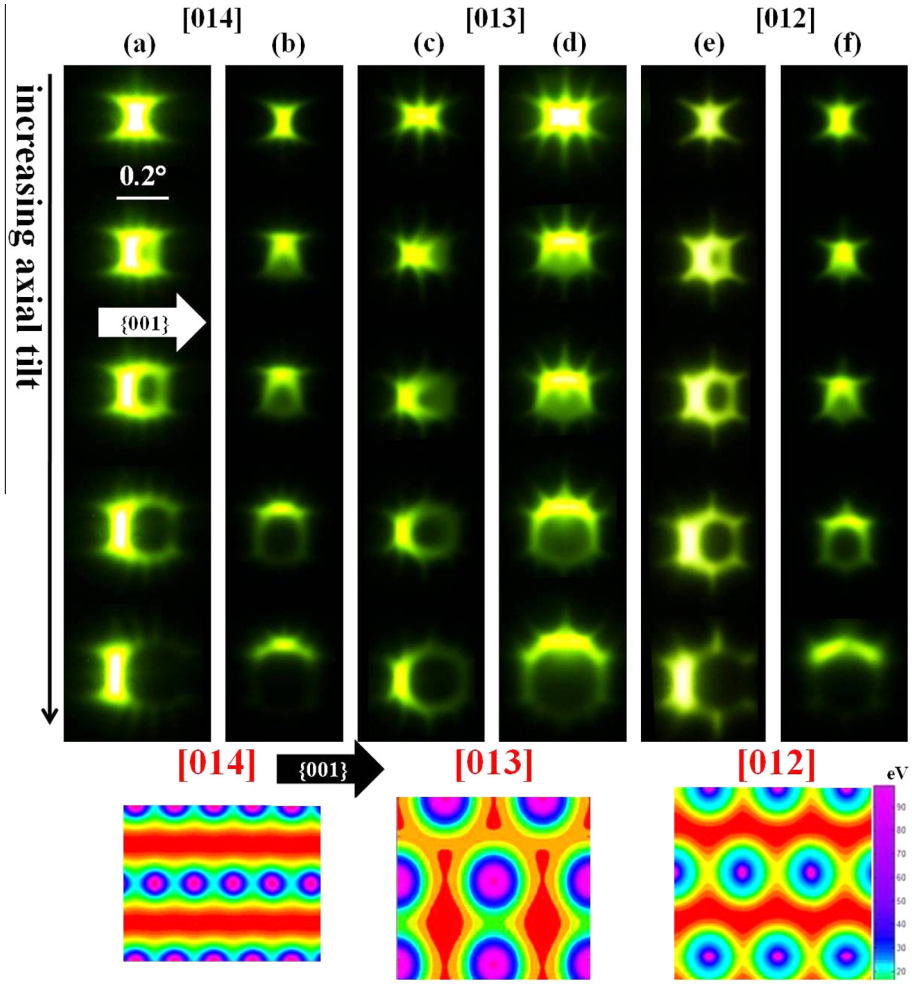

Fig. 3. Experimental channeling patterns for 2 MeV protons from a 55 nm [001] Si membrane for increasing tilts away from axes (a, b) along, orthogonal to (001) plane at [014] axis respectively, (c, d) along, orthogonal to (001) plane at [013] axis respectively, (e, f) along (001) and (112) planes from the [012] axis, in increments of $\psi_c/6$. A common scale bar has been assigned for all patterns. Lattice potential maps are shown below each axis.

[012], [014] and [113] axes, comprising a ring-like structure as observed at other hexagonal lattices, but with an additional feature of a vertical line which is observed at all tilts though is clearest around $\sim\psi_c/2$. The [114] axis incorporates two closely-spaced atoms located at each corner of the unit cell, so the vertically-running {221} lattice direction comprises atom rows with two different geometries, though their width is the same. In one row geometry atoms along the walls are offset and in the other geometry the atoms face each other. This second group gives rise to the additional feature in tilted axial channeling patterns, while the first group produces the larger, ring-like doughnut.

FLUX simulations were performed to study the origin of this additional feature. The simulated angular pattern at the [114] axis for a tilt of $\sim\psi_c/2$ is shown in Fig. 8a, which well-reproduces the experimentally recorded pattern in Fig. 4b. Three rows show different angular regions along the vertical line feature, and Fig. 8b and c shows the origin of each angular region in terms of the respective simulated entrance and exit spatial coordinates of those selected protons. One clearly sees in the top row that the vertical angular line originates from those protons which enter atom rows containing facing atoms along the {221} direction. Ions incident on this row geometry undergo a vertical deflection upwards (third row) or downwards (second row), depending on whether they are reflected from or move through the potential barrier produced by the two facing atoms.

Now consider the [112] atomic arrangement which is rectangular in shape, Fig. 2a, with a vertically-running {111} direction comprising wide and narrow planes. In both types the row atoms along the walls face each other so for the narrow planes there are two closely-spaced atoms which form a potential wall similar to that for the [114] axis. In Fig. 4f a small tilt away from the [112] axis along the vertically-running (111) planes results in a symmetric, doughnut, with a vertically-running line down the center. Fig. 9d–f respectively show FLUX simulated channeling patterns under the same conditions for the combined planes, and only wide and narrow planes respectively for a layer thickness of 65 nm. This thickness takes into account the increased path length in the recorded pattern owing to tilting the [001] crystal to the [112] axis. Clearly the central vertical feature originates from the narrow {111} planes while the channeled beam fraction which enters the wide planes produces the familiar doughnut distribution.

Fig. 9a–d shows simulated channeling patterns for the [112] axis for four different crystal layer thicknesses. The central feature changes from an inverted V-shape in Fig. 9a and b, to an upright V-shape in Fig. 9c. This change is related to a transverse oscillatory motion imparted to the beam portion which falls on the row atoms of the narrow {111} planes. The beam has transverse momentum in the vertical direction and this portion all passes between the closely-spaced atoms (separation of 0.784 Å), whereas a fraction was reflected from them for the [114] axis where the spacing is

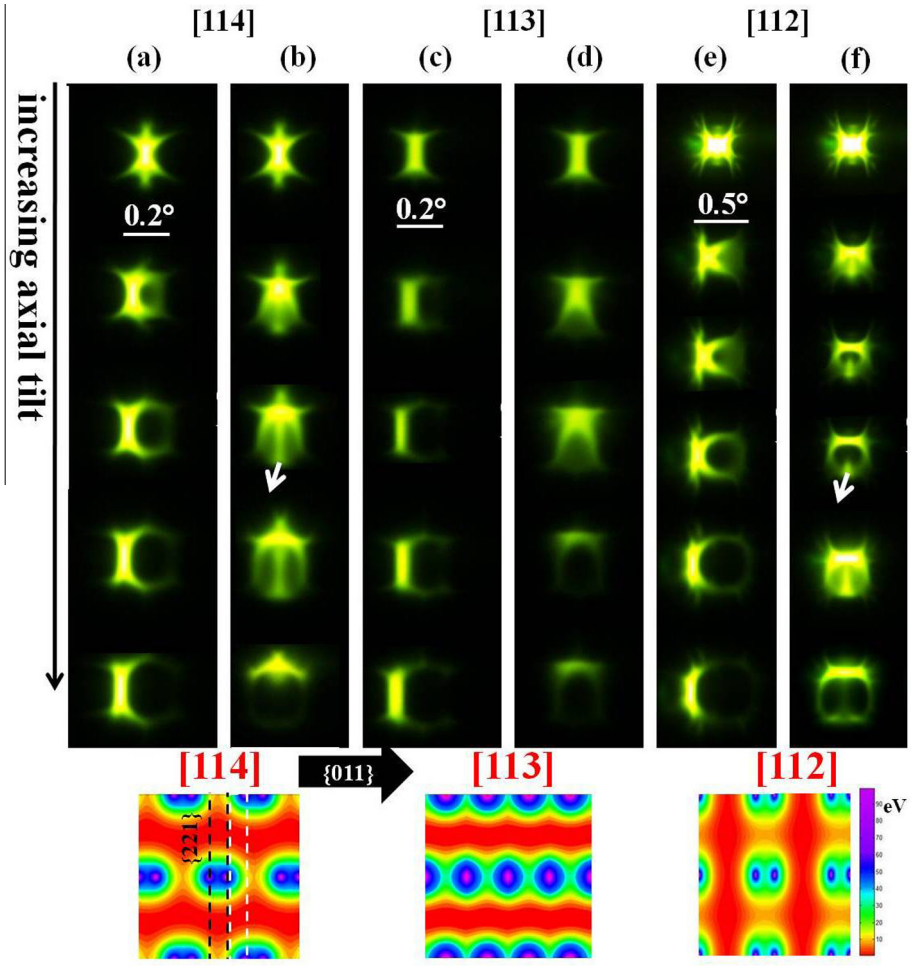

Fig. 4. Experimental channeling patterns for 2 MeV protons from a 55 nm [001] Si membrane for increasing tilts away from axes (a, b) along, orthogonal to (011) plane at [114] axis respectively, (c, d) along, orthogonal to (011) plane at [113] axis respectively, (e, f) along (011) and (111) planes from the [112] axis in increments of $\psi_c/6$. Individual scale bars are given for each axis. Lattice potential maps are shown below each axis – for the [114] axis the two different row geometries along the vertically-running {221} planes are shown.

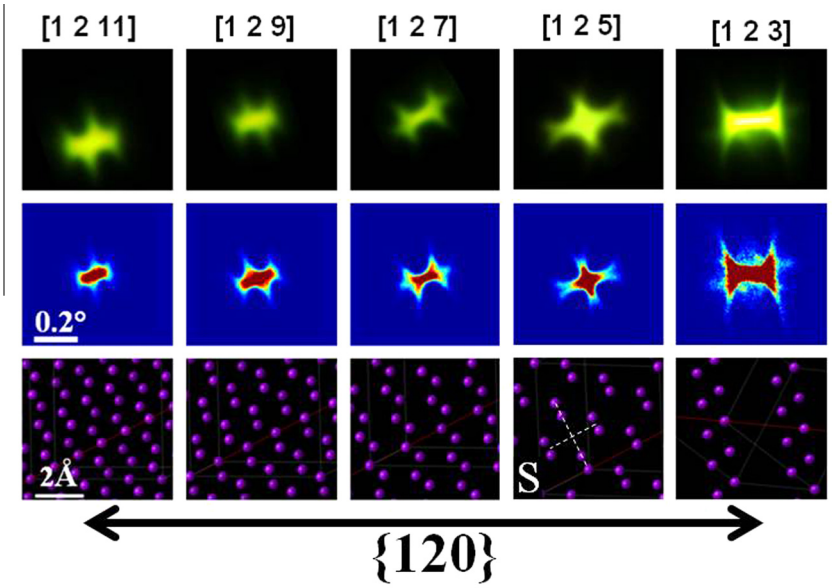

Fig. 5. Experimental and FLUX simulated angular distributions for 2 MeV protons from 55 nm thick Si membrane at minor axes along the {012} plane.

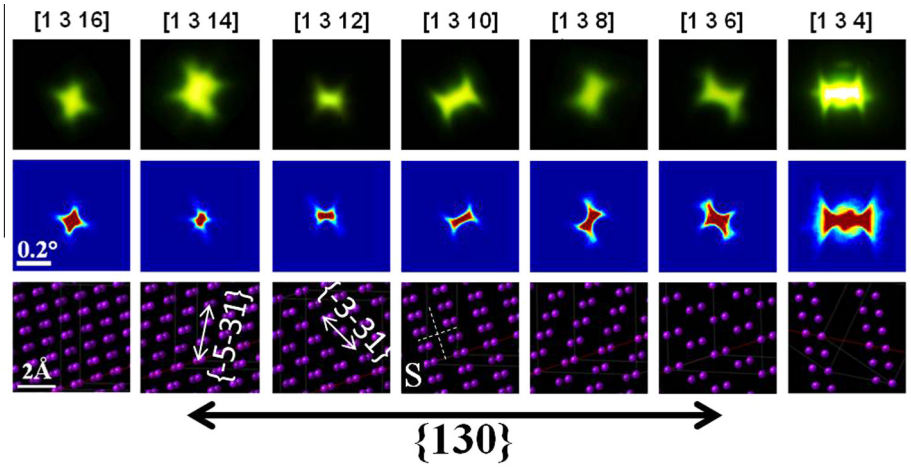

Fig. 6. Experimental and FLUX simulated angular distributions for 2 MeV protons from 55 nm thick Si membrane at minor axes along the {0 1 3} plane.

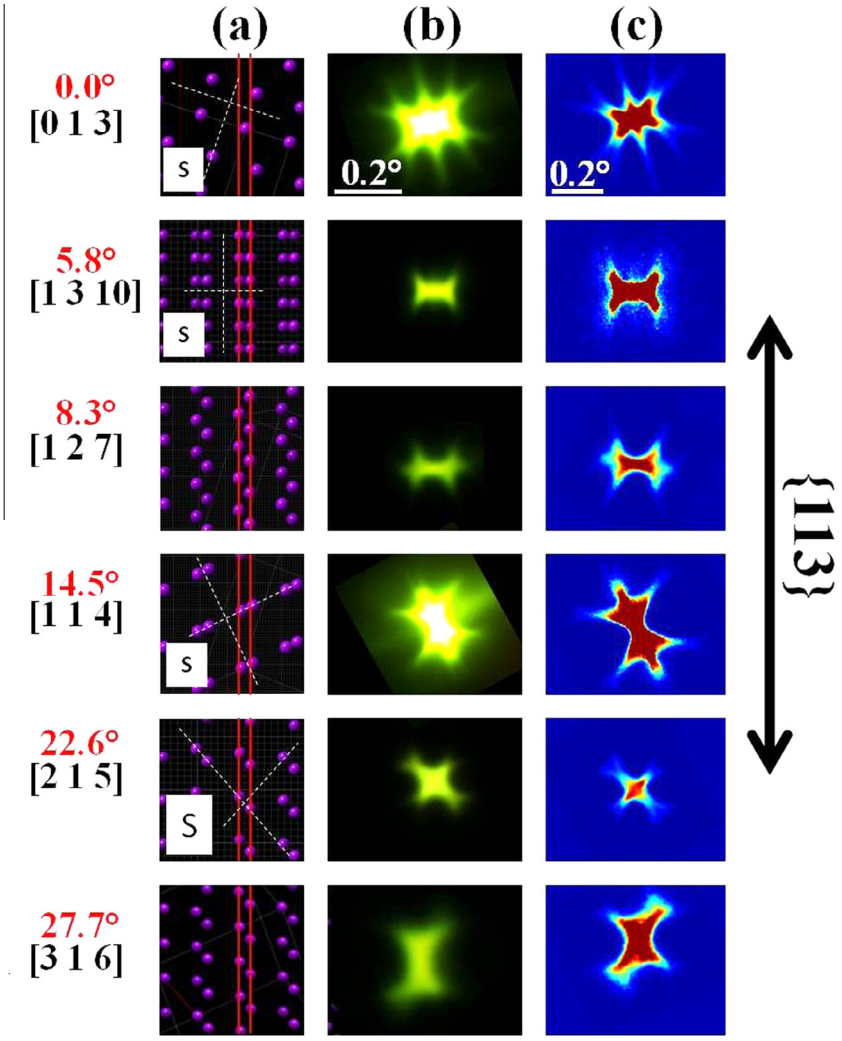

Fig. 7. (a) Axial atomic projections along a {1 1 3} plane, (b, c) experimental and FLUX simulated axial channeling angular distributions for 2 MeV protons from a 55 nm [0 0 1] Si membrane showing the asymmetry along the narrow {1 1 3} planes indicated by the red lines. (For interpretation of the references to colour in this figure legend, the reader is referred to the web version of this article.)

significantly smaller (0.452 Å). As the beam moves downwards through the gap, it is compressed to a smaller area but with a larger divergence, resulting in the oscillatory nature of this feature in the channeling pattern.

Comparing this behavior with that observed at the [2 1 3] and [3 1 4] axes [20], which also contain wide and narrow {1 1 1} planes, but the row atoms are offset, rather than facing each other as at the [1 1 2] axis. One observes a small, inner doughnut from the narrow

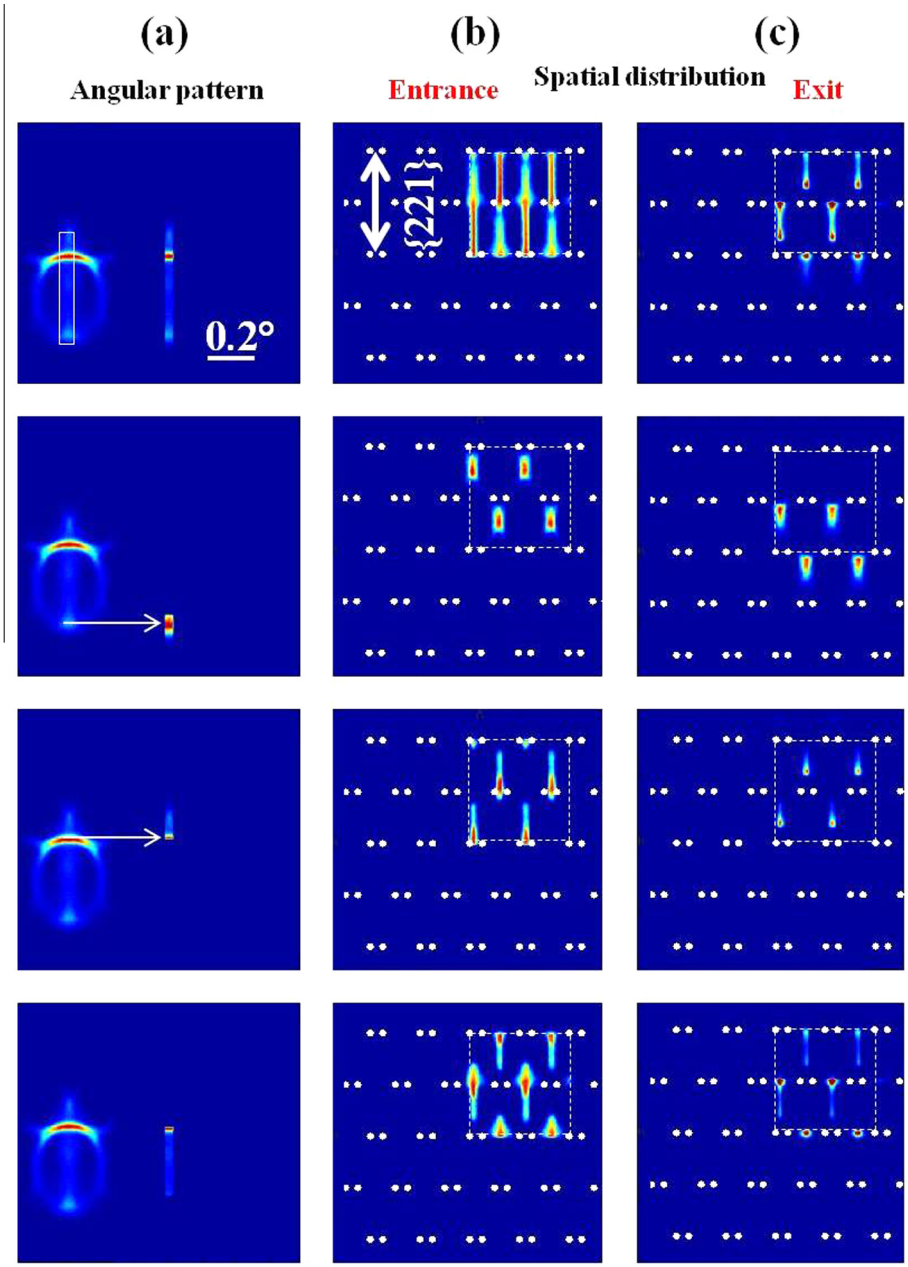

Fig. 8. FLUX simulations of the patterns at [114] axis for 2 MeV protons from a 55 nm [001] Si membrane for a tilt angle of 0.1° ($\psi_c \sim 0.18°$) along the {221} plane (b), (c) spatial coordinates (dashed box size of 3.84 Å × 3.84 Å) of the selected angular region shown in (a).

planes on tilting parallel to the {111} direction, instead of the V-shape/line feature at the [112] axis, shown in Fig. 2c. Thus, whether a doughnut or V-shape/line feature is produced as the inner feature simply depends on the orientation of the atom row of the narrow planes.

Even though their lattice row geometries are very different, the presence of two facing, closely-spaced atoms produces similar effects on the patterns observed at the [114] and [112] axes, with a distinctive feature which is clearly differentiated from the surrounding doughnut distribution. Fig. 10 shows a compendium of all recorded examples of channeling patterns for tilting the crystal perpendicular to axes comprising facing atoms. The [014] axis is also included at the right to provide an example of an axis where there are no two closely-spaced atoms. They are presented in terms of decreasing spacing between the two facing atoms, from [011] where it is large, to the [149] where it is the smallest. The patterns all comprise a central feature, which may be a V-shape for the larger atom spacing, or for smaller atom spacing, e.g. for the [114] and [149] one observes just a line. While the feature may change in width and shape, as described in Fig. 9, we conclude that for a small spacing the change in potential, and therefore the change in spatial position and transverse angle experienced by the beam portion reflected from or passing between the two atoms is smaller than for a wide spacing, so a line is more likely to be observed. Similarly, a wider V-shape is related to a larger potential and so a greater transverse angle imparted to the beam fraction as it passes between the two atoms.

It is noteworthy that one may detect an asymmetric lattice arrangement, i.e. [129] and [149], where the patterns are slightly asymmetric. Also, note the similarity between the patterns from the [112] and [1310] axes which have a similar lattice arrangement in which the narrow {111} and {113} planes respectively

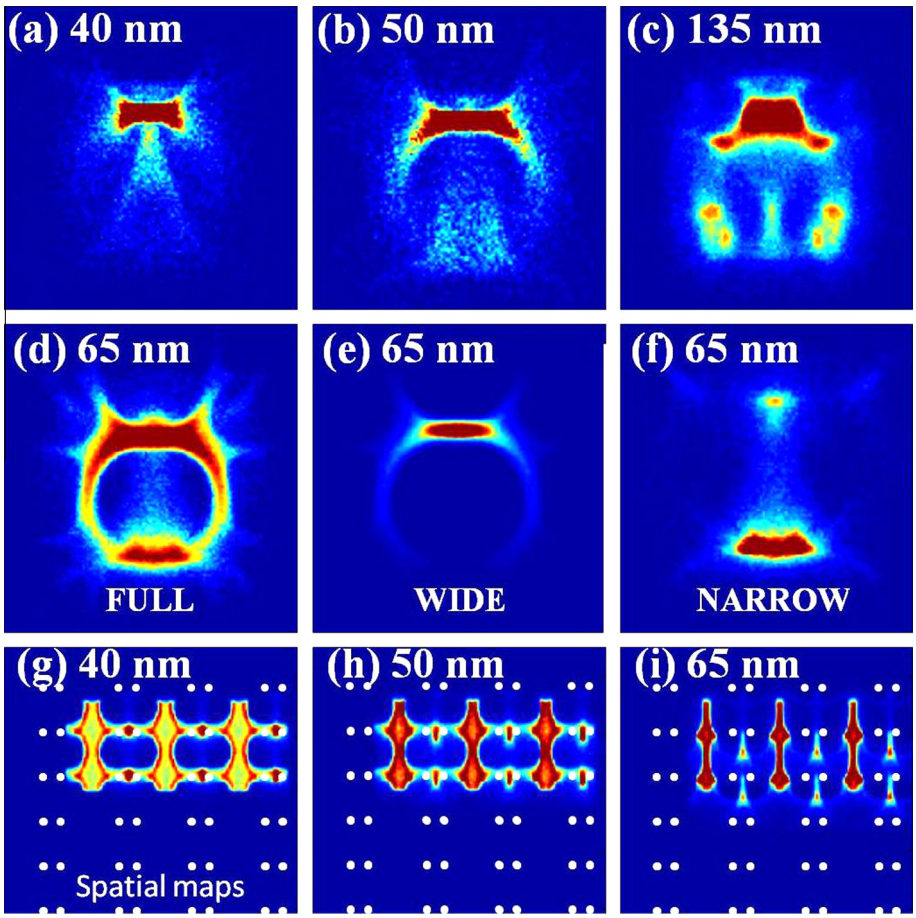

Fig. 9. (a–d). FLUX simulations of [1 1 2] axis for different layer thicknesses (note they are out of order). (d–f) Separate patterns produced by the combined planes, only the wide and only the narrow {1 1 1} planes respectively for a layer thickness of 65 nm. (g–i) Spatial maps of all protons at the layer thicknesses corresponding to (a, b, d).

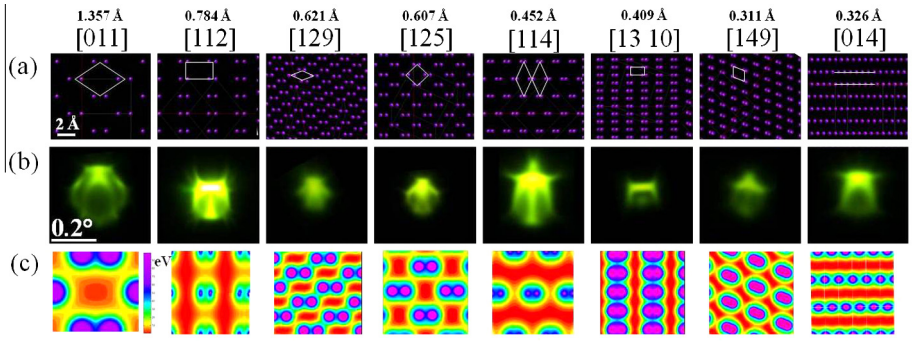

Fig. 10. Compendium of channeling patterns when tilting the crystal perpendicular to close-spaced atoms, in order of decreasing spacing between the two atoms. Note that for the [1 4 9] axis the contrast between the two atoms is saturated, see Fig. 11 for a magnified version.

have atoms facing each other, whereas the rest have a hexagonal lattice.

4.3. Pattern symmetry

Consider the symmetry of channeling patterns observed at axes with similar atomic arrangements in Figs. 2–8. A perfect correlation is observed between the lattice and pattern symmetry/asymmetry in both the experimental and simulated patterns.

Consider Fig. 7 which shows patterns from axes along the {1 1 3} direction where both the wide and narrow planes comprise offset atom rows. At the [1 2 7] and [3 1 6] axes for example, both wide and narrow {1 1 3} planes contain offset row atoms and the lattice has no planes of mirror symmetry. The corresponding channeling patterns are asymmetric. However, at the [0 1 3] and [2 1 5] axes for example, again both the wide and narrow {1 1 3} planes contain offset row atoms; but now the lattice contains symmetry directions, and so the resulting patterns are symmetric. Clearly lattice symmetry is the most important aspect in determining the resulting pattern symmetry at axial alignment, rather than whether different rows contain offset atoms at an axis.

Another interesting example is the patterns at axial alignment at the [0 1 1] in Fig. 2b, and the [1 2 5] and [1 2 1 1] axes in Fig. 5. The lattice geometry is hexagonal in each. There are two orthogonal planes of symmetry at the [0 1 1] and [1 2 5] axes, whereas the [1 2 1 1] axis is asymmetric. The patterns each comprise a similar

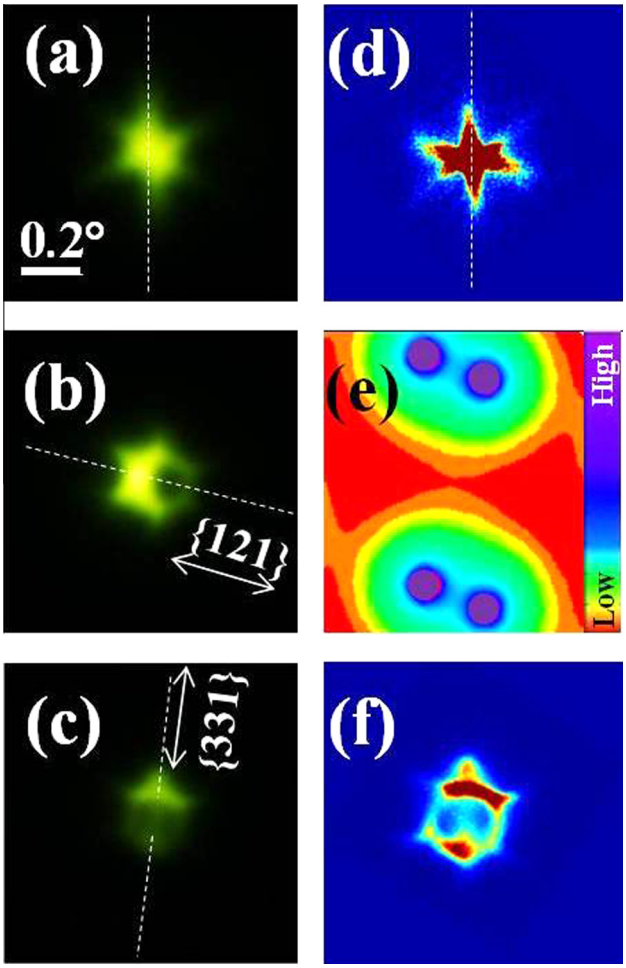

Fig. 11. Experimental doughnut patterns at the [149] axis for (a) aligned, a tilt of $\sim\psi_c/2$ along (b) {121} and (c) {331} planes for 2 MeV protons from a 55 nm [001] Si membrane. (d, f) FLUX simulations of aligned and tilted patterns corresponding to (a), (c) respectively (e) lattice arrangement at the [149] axis, presenting a magnified view of that shown in Fig. 10. Dashed lines are shown to highlight the small, but resolvable asymmetry in the patterns.

cross-structure, however those from the [011] and [125] axes are symmetric while that for the [1211] axis is not.

4.4. Deduction of the geometry of an unknown axis

To illustrate how the above compilation and analysis of features present in channeling patterns might be used to identify aspects of an unknown atomic arrangement, consider Fig. 11a–c, which shows channeling patterns recorded at the [149] axis, for (a) aligned case and tilted cases. The vertical line inner feature observed in Fig. 11c implies that this axis contains a lattice direction with two row types, one of which comprises facing atoms. In Fig. 11a and b one respectively observes a six-pointed star and a hexagonal-shape doughnut distribution, both of which imply a hexagonal lattice geometry. Considered together, one can postulate a hexagonal lattice geometry similar to many of those shown in Fig. 10. Furthermore the slight asymmetry observed in Fig. 11a and c implies that the lattice is asymmetric. All of these features are correct, according the [149] lattice geometry shown in Figs. 11e and 10 and confirmed with FLUX simulations showed in Fig. 11d and f.

4.5. Quasi-channeling phenomena

A further point of interest is to consider how narrow an inter-atomic spacing one can detect using this mode of observation of ion channeling phenomena. In Fig. 11 the vertically-running {331} planar inter-atomic spacing is 0.311 Å, slightly less than twice the ZBL screening radius of 0.33 Å (2×0.165 Å) [25]. Therefore, we conclude that we are observing channeling phenomena which are within the screening radius, previously referred to as quasi-channeling [3,10]. Such a small planar width is only visible in channeling patterns at the very early stage of the ion trajectory. We believe that this is the first observation of channeling-related phenomena from lattice spacings which are less than the screening radius.

5. Conclusion

We have presented a compendium of transmission channeling patterns from major and minor axes near the silicon [001] axis. They exhibit symmetric or asymmetric features based on their lattice geometry. Axes containing a lattice direction with identical rows produce a simple doughnut distribution at a small tilt. In comparison, axes which incorporate atom rows with different spacings or different row geometries produce a more complex channeling pattern comprising an outer doughnut and an inner feature produced by beam incident on either narrower atom rows or those which contain facing, rather than offset atoms. For the first time we reported the quasi-channeling angular patterns from the planar widths which are less than the screening radius.

References

[1] D.S. Gemmell, Rev. Mod. Phys. 46 (1974) 129.
[2] J. Lindhard, Phys. Lett. 12 (1964).
[3] L.T. Chadderton, Radiat. Effects 27 (1975) 13.
[4] R.B. Simonton, C.W. Magee, A.F. Tasch, Nucl. Instrum. Methods Phys. Res. Sect. B Beam Interact. Mater. Atoms 74 (1993) 142.
[5] R.G. Wilson, J. Appl. Phys. 52 (1981) 3985.
[6] J.F. Ziegler, R.F. Lever, Appl. Phys. Lett. 46 (1985) 358.
[7] J. Remillie, J.J. Samueli, A. Sarazin, J Phys 28 (1967).
[8] Lt. Chaddert, F.H. Eisen, Philos. Mag. 20 (1969).
[9] D.S. Gemmell, R.E. Holland, Phys. Rev. Lett. 14 (1965) 945.
[10] G. Dearnaley, I.V. Mitchell, R.S. Nelson, B.W. Farmery, M.W. Thompson, Phil. Mag. 18 (1968) 985.
[11] M.B.H. Breese, P.J.C. King, P.J.M. Smulders, G.W. Grime, Phys Rev B 51 (1995) 2742.
[12] M.B.H. Breese, P.J.C. King, G.W. Grime, P.J.M. Smulders, L.E. Seiberling, M.A. Boshart, Phys Rev B 53 (1996) 8267.
[13] Z.Y. Dang, M. Motapothula, Y.S. Ow, T. Venkatesan, M.B.H. Breese, M.A. Rana, A. Osman, Appl. Phys. Lett. 99 (2011) 223105.
[14] V. Guidi, A. Mazzolari, D. De Salvador, L. Bacci, Phys. Rev. Lett. 108 (2012) 014801.
[15] J.S. Rosner, W.M. Gibson, J.A. Golovchenko, A.N. Goland, H.E. Wegner, Phys. Rev. B 18 (1978) 1066.
[16] Lt. Chaddert, J. Appl. Crystallogr. 3 (1970).
[17] S.K. Andersen et al., Nucl. Phys. B 167 (1980) 1.
[18] M. Motapothula, Z.Y. Dang, T. Venkatesan, M.B.H. Breese, M.A. Rana, A. Osman, Phys. Rev. Lett. 108 (2012) 195502.
[19] M. Motapothula, Z.Y. Dang, T. Venkatesan, M.B.H. Breese, M.A. Rana, A. Osman, Nucl. Instrum. Methods Phys. Res. Sect. B Beam Interact. Mater. Atoms 283 (2012) 29.
[20] D.D. Armstrong, W.M. Gibson, H.E. Wegner, Radiat. Effects 11 (1971) 241.
[21] M. Motapothula, S. Petrović, N. Nešković, Z.Y. Dang, M.B.H. Breese, M.A. Rana, A. Osman, Phys. Rev. B 86 (2012) 205426.
[22] D. Borka, S. Petrovic, N. Neskovic, J. Electron Spectrosc. Relat. Phenom. 129 (2003) 183.
[23] J.P. Biersack, J.F. Ziegler, Nucl. Instrum. Methods Phys. Res. 194 (1982) 93.
[24] P.J.M. Smulders, D.O. Boerma, Nucl. Instrum. Methods Phys. Res. Sect. B 29 (1987) 471.
[25] G. Hobler, Radiat. Eff. Defects Solids 139 (1996) 21.